Materials Advances

ROYAL SOCIETY OF CHEMISTRY

PAPER

View Article Online
View Journal | View Issue

Cite this: *Mater. Adv.*, 2022, 3, 6628

A novel flame-resistant separator for high performance lithium–sulfur batteries†

Jianyi Wang,‡[a] Menghui Chen,‡[b] Weiwei Qin *[ac] and Meng Zhou [c]

Lithium–sulfur batteries (LSB) offer a high energy density in energy storage systems in the long run, and are of much lower cost than commercially available lithium-ion batteries. The electrochemistry performance of LSB can be improved greatly through the electro-catalytic mechanism, especially when it is applied on the separator, facing towards the cathode. However, due to the limitations of current technology (vacuum filtration and the slurry coat on polypropylene), high performance LSB's development is stunted. In this paper, an ultra-thin coating and quick methods were investigated to improve the performance of LSB by a synergy between a reduced graphene oxide (RGO) loaded S-catalyst (O-vacancy-enriched $-BaTiO_3$) and glass fiber separator, which has excellent fire retardant and high temperature performance (cycled more than 100 times at 60 °C), and can greatly prolong the service life of the LSB. The following theories and experiments show that the original separator modified design produces the electrochemical and safety performance of the LSB, which is significant for both theoretical research and vast application prospects.

Received 23rd May 2022,
Accepted 26th June 2022

DOI: 10.1039/d2ma00576j

rsc.li/materials-advances

1. Introduction

With the development of various electric vehicles and electronic products, the existing commercial lithium-ion battery (LIB) can no longer answer the needs of people's requirement for high energy and low-cost batteries. Among battery systems, due to the low price and wide range of resources, lithium–sulfur batteries (LSB) have broad application prospects for energy storage. Also, because of the low molecular weight of sulfur and the multi-electron redox reaction, LSB have a very high energy density (2600 W h kg^{-1}) and theoretical specific capacity (1,675 mA h g^{-1}).[1] LSB are considered as the most promising next-generation battery systems that can achieve both cost effectiveness and energy density. However, LSB have some serious problems, such as the insulation of sulfur and Li_2S, a shuttle effect caused by polysulfide dissolution and shuttle, and lithium dendrite growth.[2,3] To address the existing problems of LSB, researchers have expended a lot of effort and made some progress. At present, the work is mainly focused on the composite cathode and artificial three dimensions (3D) current collector. However, the modification of the separator is also an important part of the battery, because it plays a great role in the electrochemical performance.

The main components of Celgard series separators are polypropylene (PP) and polyethylene (PE), which hardly limit the diffusion of polysulfide. The reason is that, because of its large pore size, polysulfide can pass through easily by electric field drive and concentration difference between the cathode and anode areas.[4,5] At present, there are great challenges in the interface structure design and surface modification of lithium metal anodes. The separator modifications include special mechanisms to inhibit lithium dendrite formation and polysulfide diffusion, which is expected to promote the development and practical application of LSB.[6,7] In addition, most research focuses on the modification of PP separators, which can hinder the diffusion of polysulfide and improve the performance of LSB (Scheme 1a).[8] Functional design of the modified separator is one of the feasible and simple methods to improve the performance of LSB. So far, many new functional separators have shown great potential in practical battery applications. By introducing functional materials coatings on the separator, including polymer materials, carbon-based materials,[9–12] inorganic oxides,[13,14] catalytic polar metal compounds[15] and metal/covalent organic frameworks,[16–20] the specific capacity, cycle stability, multiplier performance, Coulomb efficiency and safety of LSB can be significantly improved. There are two main preparation technologies: one is to use the vacuum suction filtration and barrier layer which were placed on the surface of the PP separator, but this method takes a long time, especially for nanomaterials; the other one

[a] *Faculty of Geosciences and Environmental Engineering, Southwest Jiaotong University, Chengdu 611756, China. E-mail: weiwei.qin@swjtu.edu.cn*
[b] *Institute for Sustainable Energy/College of Sciences, Shanghai University, Shanghai, 200444, China*
[c] *Chemical and Materials Engineering Department, New Mexico State University, Las Cruces, NM, 88003, USA*

† Electronic supplementary information (ESI) available. See DOI: https://doi.org/10.1039/d2ma00576j

‡ These authors contributed equally.

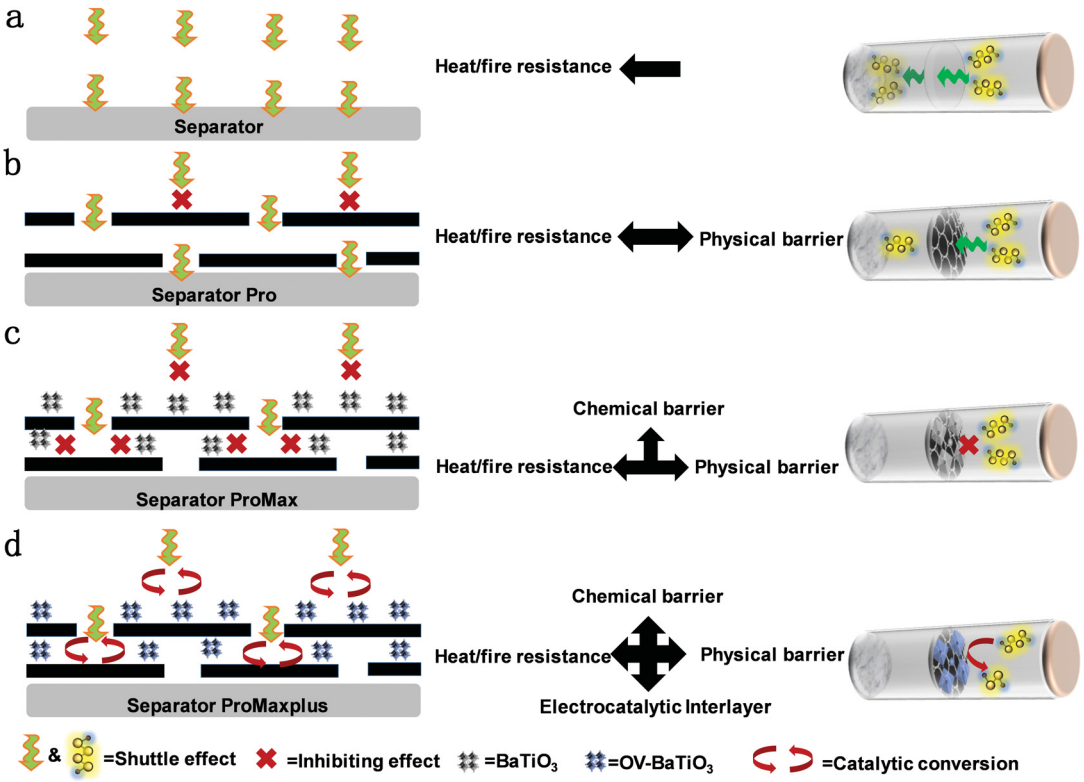

Scheme 1 Schematic illustration of the different designs of separator for lithium–sulfur batteries.

would be make a paste of barrier with binder and coat on the PP separator, yet the thickness of the layer cannot be controlled. Therefore, developing a new type of preparation technology which can integrate the advantages of composite separators and get rid of their disadvantages is of critical importance.

In addition, the thermal safety of LSB is particularly important due to the use of lithium metal anodes and sulfur cathodes.[21] At present, thermal safety research in the field of LSB is in urgent need of further research. Most of the existing modified coating separators are based on PP separator modifications, so their thermal stability is poor.[22] Therefore, choosing glass fiber membranes for sodium ion batteries presents a price advantage[23] and their good heat resistance as separator has great advantages. In addition, it is essential to hinder the diffusion of polysulfide so it is trapped in cathode area and reactivate the deposition of deactivated sulfur-containing substances, which enhance the utilization active material. The modified coating separator applied to LSB not only needs to have properties of electrostatic repulsion, steric resistance, physical and chemical adsorption and other ways to control the polysulfide, but also needs to combine with the conductive medium to reduce the interface resistance between the cathode and separator, so as to effectively improve the utilization rate of active substances in the cathode area. Recently, a novel composite cathode material ($LiFePO_4$/graphite) for dual-ion batteries has been proposed. The composite cathode combines LFP, with high capacity and high stability, and graphite, with high conductivity and high voltage, showing excellent electrochemical performance.[24] In addition, carbon nanotubes are combined with transition metal selenides. Carbon nanotubes have good conductivity, forming a network structure in the composite electrode, and enhance the specific capacitance of the charge path with good conductivity.[25] By far the most successful example of carbon-incorporation-enhanced battery performance is graphene.[26] The typical short-tubular antimony trithiophosphate $SbPS_4$ composite with graphene oxide ($SbPS_4$/GO) exhibits a high theoretical specific capacity according to the dual mechanism of transformation alloying. Inserting a unique short tube into the composite can promote the transport of Na ions, alleviate the huge volume change during charge and discharge, and improve the chemical performance.[27] If graphene was applied in LSB, the charge transfer resistance would be reduced, the utilization rate of the electrode active material would be improved, and the energy density of battery would be increased.[28]

In this paper, a reduced graphene oxide supported oxygen vacancy enriched $BaTiO_3$ (OV-$BaTiO_3$@RGO) was selected as the separator coating because the pure carbon material is not fully encapsulated in the separator and has cracking and fracture sites, preventing conventional carbon materials from capturing polysulfide (Scheme 1b). In this regard, the strategies of ferroelectric barium titanate ($BaTiO_3$) as an additive[29] and PP separator coating[30] have been proved. However, it is difficult to suppress the polysulfide filling within the structure of RGO and each particle (Scheme 1c). In general, the long-term cycling performance of LSB remains to be improved. The mixture of

OV-$BaTiO_3$@RGO with ethanol is uniformly loaded on the surface of the glass fiber diaphragm by a suction filtration method to improve the conductivity and utilization of S. The oxygen vacancy of OV-$BaTiO_3$ with ferroelectricity and electrocatalytic activity as a separator coating achieves a synergy with fixed soluble polysulfide and a catalytic effect, which can be the further adsorption of polysulfide dissolved in the electrolyte, and provides the active material sulfur with electrochemical reactivity to increase the specific capacity (Scheme 1d). Reduced capacity decays by 0.09% during the cycle (1 A g^{-1}). An excellent reversible capacity of 720 mA h g^{-1} was obtained after 200 cycles, even with a high sulfur content (90%) and load (10 mg cm^{-2}) and a high area capability of 7 mA h $cm^{-2}$was maintained. In order to reveal the mechanism of the electrochemical reaction, a series of electrochemical experiments were carried out. *In situ* XRD results show that there is a strong interaction between the charge and discharge products of S during cycles, and the CV results of the polysulfide symmetric battery also confirmed the catalytic effect on Li_2S. Combined with theoretical calculations (DFT), we found that the dynamic change process has a strong effect on polysulfide with OV-$BaTiO_3$. In addition, the modified glass fiber separator can not only achieve the ideal flame retardant effect, but also maintain the excellent electrochemical performance of LSB.

2. Experimental section

2.1 Materials

All chemical materials are commercially available and were used without further purification: barium titanate ($BaTiO_3$, 99.9% metals basis, <100 nm), reduced graphene oxide (rGO), sodium (99.7%, storage in kerosene), potassium (99%, storage in kerosene), 1-methyl-2-pyrrolidinone (NMP, 99.5%), poly(vinylidene fluoride) (average Mw ~400 000), sublimed sulfur (99.95% metals basis, powder), ethanol (99.5%, industrial-grade). The carbon-coated aluminum foil, lithium plate, electrolyte (1.0 M LiTFSI in DOL : DME = 1 : 1 Vol% with 2.0% $LiNO_3$) and GF separator were purchased from **https://www.canrd.com**.

2.2 Synthesis of OV-$BaTiO_3$

The 50 mL beaker was stirred gently together with the nanoparticles of $BaTiO_3$ and Na–K alloy until there was no visible white and the excess of Na–K alloy was removed with DMC and pure water. Then the sample (OV-$BaTiO_3$) was put in a vacuum drying oven to be dried (Fig. S7a, ESI†). XRD patterns show that the OV-$BaTiO_3$ is well-crystallized (Fig. S7b, ESI†). Meanwhile the oxygen vacancy was tested by Electron Paramagnetic Resonance (EPR, Fig. S7c, ESI†) spectroscopy and an obvious peak is shown. An amorphous interface shows in HR-TEM, which further explains the appearance of the $BaTiO_3$'s surface (Fig. S7d, ESI†). The particle size of OV-$BaTiO_3$ is about 60 nm. It should be noted, it is hard to tell the difference between the two materials of $BaTiO_3$ and OV-$BaTiO_3$ by high-resolution X-ray photoelectron spectroscopy (XPS) spectroscopy (Fig. S8, ESI†).

It was found using EPR that the OV-$BaTiO_3$ from alkali metal reducing agent assisted fabrication keeps high amounts of oxygen vacancies, which increases ion transport in Li–S battery systems. The introduction of oxygen vacancies can change the electron band structure of the polysulfide catalyst, enhance the binding with polysulfide, and accelerate the surface electron exchange for a rapid electrochemical reaction rate.[31] In addition, the surface of oxygen vacancies provides highly active adsorption sites for diverse polysulfides and can increase the utilization rate of the S cathode.

2.3 Visible adsorption observation

The sulfur and Li_2S with a ratio at 3 : 1 were added to DOL/DME solvent followed by stirring at 25 °C for 48 h in an Argon-filled glove box, and the Li_2S_6 (polysulfides) solution could be obtained. 50 mg OV-$BaTiO_3$@RGO, $BaTiO_3$@RGO and RGO were dispersed individually in 15 mL polysulfides solutions, respectively. The changes were recorded after standing for one day.

2.4 Battery separator preparation

The preparation of the OV-$BaTiO_3$@RGO@GF separator was as follows: the OV-$BaTiO_3$ (10 mg) and RGO (10 mg) were put in a small beaker with alcohol (300 mL) under ultrasonic dispersion of 20 min. Then the process of vacuum filtration with 50 mL per GF separator was done and dried in vacuum (60 °C) and the layer was ultrathin with a thickness of 10 μm (Fig. 1d and e). The preparation of the $BaTiO_3$@RGO@GF separator and RGO@GF separator was done by same steps.

2.5 Materials characterization

The microstructure was characterized using Scanning Electron Microscopy (SEM, ZEISS Gemini 300, gold-sprayed), SEM-EDS (OXFORD Xplore), Transmission Electron Microscopy (TEM, Tecnai TF20), X-ray diffraction (XRD, BRUKER D8 ADVANCE, Cu Ka radiation), and electron paramagnetic resonance (EPR, BRUKER), respectively.

2.6 Electrochemical performance test

Firstly, the S-slurry (S : super P : PVDF = 8 : 1 : 1 with NMP) was applied to the carbon-coated aluminum foil surface, and then was dried under vacuum (60 °C). After that, the pasted aluminium foil was cut into tiny wafers (sulfur loadings of Li–S batteries are 1–2 mg cm^{-2}). The assembled battery was based on previous work[32] and the model was Li/modified separator/S. The LSB battery performance was tested in a LAND CT3002A Li-Ion battery testing system and Ivium-N-stat electrochemical workstation.

2.7 Calculation method

The Vienna *Ab initio* simulation package (VASP) was used for all density functional theory (DFT) calculations within the generalized gradient approximation (GGA) using the Perdew–Burke–Ernzerhof (PBE). The projected augmented wave (PAW) potential was chosen to describe the ion nucleus and a plane wave basis was used with a kinetic cutoff of 400 eV to consider

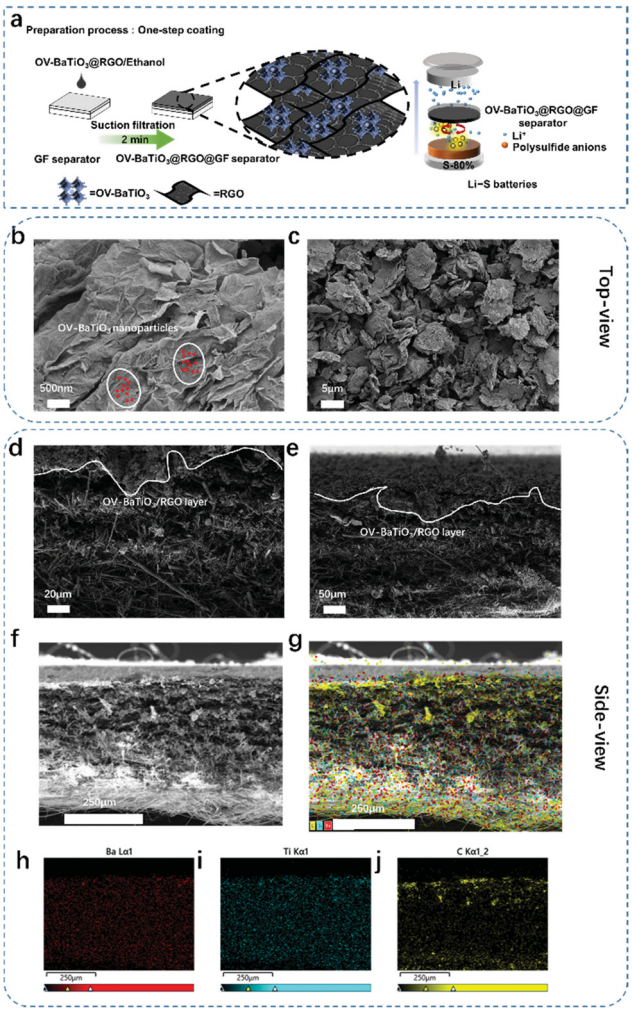

Fig. 1 (a) Schematic illustration of the preparation process of the OV-$BaTiO_3$@RGO@GF separator for lithium–sulfur batteries. The microstructure of OV-$BaTiO_3$@RGO@GF separator. (b and c) Top-view SEM images of different scales of OV-$BaTiO_3$@RGO@GF separator. (d and e) Side-view SEM images of OV-$BaTiO_3$@RGO@GF separator. (f–j) EDS elemental mapping of Ba (h), Ti (i) and C (j), and color overlay of Ba, Ti and C (g).

the valence electrons. The geometric optimization was carried out when the force convergence is less than 0.05 eV A^{-1}. 2 × 2 × 1. The Monkhorst–Pack *K*-points were used for all calculations. Two layers of atoms (45 atoms) are fixed in all calculations. Lattice parameters: a = 12.01337 Å, b = 12.60191 Å, c = 27 Å, α = 90°, β = 90°, γ = 90°.

The adsorption energy can be calculated as follows: $E = E(\text{slab} + Li_2S_x) - E\,(\text{slab}) - E\,(Li_2S_x)$.

3. Results and discussion

Fig. 1a shows the OV-$BaTiO_3$@RGO@GF separator preparation process and LSB assembly process. Using OV-$BaTiO_3$ and RGO as a coating layer is a universal method for preparing a conducting medium with high adsorption and catalysis of the surface for polysulfide anchoring. Using ethanol, vacuum filtering helps to improve the quality and efficiency of the stable coating (the process should only take 2 minutes.). Other elements and the OV-$BaTiO_3$@RGO@GF separator were subsequently joined to the LSB. Through this design we hope that our vision could become a reality, with excellent performance, and strong suppression of polysulfide in the cathode area. The process of the coating of the OV-$BaTiO_3$@RGO@GF separator was analysed using a Scanning Electron Microscope (SEM). From the top-view (Fig. 1b and c), the GF separator is coated with a uniform OV-$BaTiO_3$@RGO layer by the vacuum filter method. In addition, Fig. 1b shows that the surface of RGO has an obvious grain structure, which demonstrates that OV-$BaTiO_3$ is distributed evenly on the surface of the RGO (the corresponding regions of OV-$BaTiO_3$ nanoparticles are marked in red) without agglomeration. The OV-$BaTiO_3$ evenly dispersed on RGO is conducive to trapping soluble polysulfide which can be chemisorbed or physically absorbed on solid OV-$BaTiO_3$@RGO. Meanwhile, RGO as a secondary current collector with high conductivity and transmission and low resistance will accelerate the electrochemical reaction for the insulated S cathode. Side view of the SEM images (Fig. 1d and e) showed that the OV-$BaTiO_3$@RGO@GF separators are made predominantly of GF separator and contain an ultra-thin coating on the top of the GF separator. These are even more proof that through this design we can obtain thin-modified-separators faster. X-ray patterns of Ba, Ti and C elements in the OV-$BaTiO_3$@RGO@GF separator were detected and Ba and Ti were evenly distributed in the structure of modified separator (Fig. 1f–j). In addition, the C is at opposite ends of the separator, which suggests that the RGO in ethanol is blocked on the surface of the GF separator, and then OV-$BaTiO_3$ and ethanol can be shuttled *via* the holes of three dimensional of GF separator.

In situ XRD technology is an important method in current energy storage research analysis.[33] It cannot only eliminate the impact of external factors on the electrode material (compare with the *ex situ* XRD), but also improve the authenticity and reliability of the data when monitoring of the process of the electrochemical reaction in real-time for characterizing the structure and composition change. Thus, the whole reaction of the system can be analysed and processed more clearly, and its intrinsic reaction mechanism can be revealed. Therefore, the introduction of *in situ* XRD characterization technology can improve the understanding of the reaction features of the catalytic conversion of liquid polysulfide (shuttle factor) to solid polysulfide, which characterizes the charge–discharge process of OV-$BaTiO_3$ as the electrocatalyst layer of LSB and to explore its reaction mechanism, as shown in Fig. 2a. Through the characterization, the formation of Li_2S is confirmed. However, with the standard pure cellgard separator as a reference it can be seen that S8 peaks exist over the whole cycle of the battery test, indicating that the shuttling of polysulfides is serious.[34] Strengthening the chemical adsorption of the oxygen vacancies and permanent electric polarization of OV-$BaTiO_3$ and polysulfide is the key to improving the cyclic stability of LSB. Through "chemical adsorption" between nanoparticles of OV-$BaTiO_3$ and soluble polysulfide during the

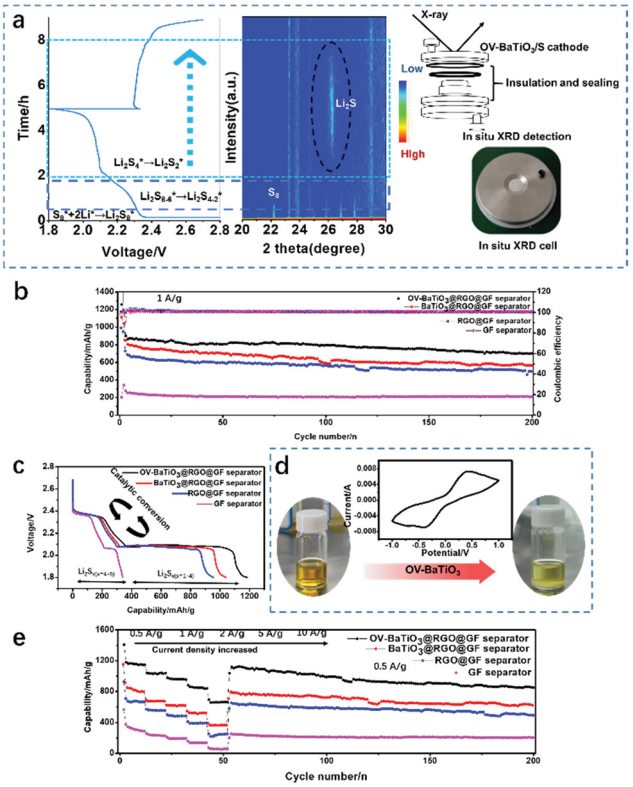

Fig. 2 (a) *In situ* XRD contour plot of the OV-$BaTiO_3$/S cathodes with the corresponding discharge–charge curves and the diffraction intensity chart on the left, the model is on the right. (b) Cycling performance of OV-$BaTiO_3$@RGO@GF separator, $BaTiO_3$@RGO@GF separator, RGO@GF separator and GF separator at a rate of 1 A g^{-1} for 200 cycles. (c) Typical discharge curves of batteries with OV-$BaTiO_3$@RGO@GF separator, $BaTiO_3$@RGO@GF separator, RGO@GF separator, and GF separator at a rate of 0.2 A g^{-1}. (d) Visualized adsorption of Li_2S_6 by pristine OV-$BaTiO_3$ (CV curves of the symmetric cells with cathode of OV-$BaTiO_3$ in an electrolyte with Li_2S_6 at 10 mV s^{-1} is on the top). (e) The rate capability of LSB from 0.5 to 10 A g^{-1}.

charging and discharging process, insoluble products that cannot be dissolved in the electrolyte are formed, to effectively inhibit the loss of active substances.

The cathode using the pure S electrode (without C/S composite material) combined with the OV-$BaTiO_3$@RGO@GF separator has highest performance at the same current density. The initial capacities of LSB with OV-$BaTiO_3$@RGO@GF separator, $BaTiO_3$@RGO@GF separator, RGO@GF separator and GF separator at 1 A g^{-1} current density are 897, 849, 720 and 273 mA h g^{-1} (Fig. 2b), respectively. Moreover, it can be seen that the LSB with the OV-$BaTiO_3$@RGO@GF separator cycled 200 cycles retains a capacity of 720 mA h g^{-1}, with a low-capacity decay of 0.08% per cycle. These results indicate that OV-$BaTiO_3$ is able to effectively inhibit the shuttle effect and reduce the polysulfide shuttle. Its unique properties of oxygen vacancy provide a driving force for polysulfide conversion and accelerate the electrochemical kinetics process. Then the mechanism of OV-$BaTiO_3$'s specific contribution to battery capacity is explored. It can be further seen from the variation of the voltage–capacity curve that the LSB with a OV-$BaTiO_3$@RGO@GF separator has a significantly higher discharge capacity from Fig. 2c.

At the end of the charge–discharge cycles test, the battery is tested using an electrochemical impedance spectrum (EIS) and the result shows that OV-$BaTiO_3$@RGO@GF separators have a low-impedance (Fig. S1, ESI†). These tests are a further demonstration that oxygen vacancy has outstanding abilities. In addition, the infiltration experiment further proved the adsorption effect of OV-$BaTiO_3$ with polysulfide (Fig. 2d). The CV curve of the Li_2S_6 symmetric battery shows that OV-$BaTiO_3$ electrode has good reversibility and fast redox kinetics, indicating that the inherent electrochemical activity of OV-$BaTiO_3$ can effectively accelerate the redox kinetics of active substances. In addition, from the adsorption experiment (Fig. S2, ESI†), the color change of OV-$BaTiO_3$@RGO after adsorbing Li_2S_6 was the most obvious (compared with $BaTiO_3$@RGO and RGO), which further indicated that OV-$BaTiO_3$@RGO had strong adsorption performance for Li_2S_6. The above results showed that O-vacancy-enriched $BaTiO_3$ could effectively adsorb polysulfides under the synergistic effect of O-vacancy and ferroelectricity, and effectively inhibit the shuttle effect. The influence of catalytic conversion is more significant in the presence of OV-$BaTiO_3$ compared with RGO (Fig. S3, ESI†). In the study of rate performance (Fig. 2e), the discharge capacities of LSB with OV-$BaTiO_3$@RGO@GF separators at 0.5–10 A g^{-1} are 1184, 1048, 986, 882 and 693 mA h g^{-1}, respectively. The physisorption and chemisorption without catalytic conversion of the $BaTiO_3$@RGO@GF separator is only 388 mA h g^{-1} at 10 A g^{-1}. These results indicate that the LSB with OV-$BaTiO_3$@RGO@GF separator has some distinct advantages for improving the capacity attenuation caused by the shuttle effect, but it can guarantee the polysulfide does not shuttle to the anode and effectively improves the utilization rate of sulfur at ultra-high current density. Under the condition of 2 A g^{-1} (Fig. S4, ESI†), the LSB with the OV-$BaTiO_3$@RGO@GF separator maintains a reversible capacity of 410.6 mA h g^{-1} at 400th cycle. The decay rate is as low as 0.06% per cycle (382 mA h g^{-1} after 600 cycles). Finally, when the surface load of S was further increased to about 10 mg cm^{-2} (Fig. S5, ESI†), the LSB had a considerable initial capacity (1358 mA h g^{-1}, 13.58 mA h cm^{-2}) at 0.05 A g^{-1}. In addition, after 18 cycles at 0.2 A g^{-1}, it can still maintain a reversible capacity of approximately 724 mA h g^{-1} (7.24 mA h cm^{-2}), which is higher than the recommend ideal LSB area capacity.[35]

In the DFT examination of battery materials, ion/molecule adsorption energy is often calculated. By comparing the adsorption energy with that of the active material, the performance of electrode materials can be estimated, and then the final theoretical results and the experimental data can be compared and analyzed.[36] Many LSB systems have been researched to solve the problems of the dissolution and shuttling of polysulfide with DFT calculations and to analyse the adsorption capacity of polysulfide on the substrate. Therefore, the adsorption energies between polysulfide and OV-$BaTiO_3$ and $BaTiO_3$ were simulated by the DFT method (Fig. 3a). The adsorption energies of OV-$BaTiO_3$ on S_8, Li_2S_8, Li_2S_6, and Li_2S_4 were −4.083, −5.782, −5.481 and −3.973 eV, respectively, indicating that the adsorption of OV-$BaTiO_3$ on LiPSs was achieved by the OV–S bond, which was consistent with the expected results. Although the adsorption

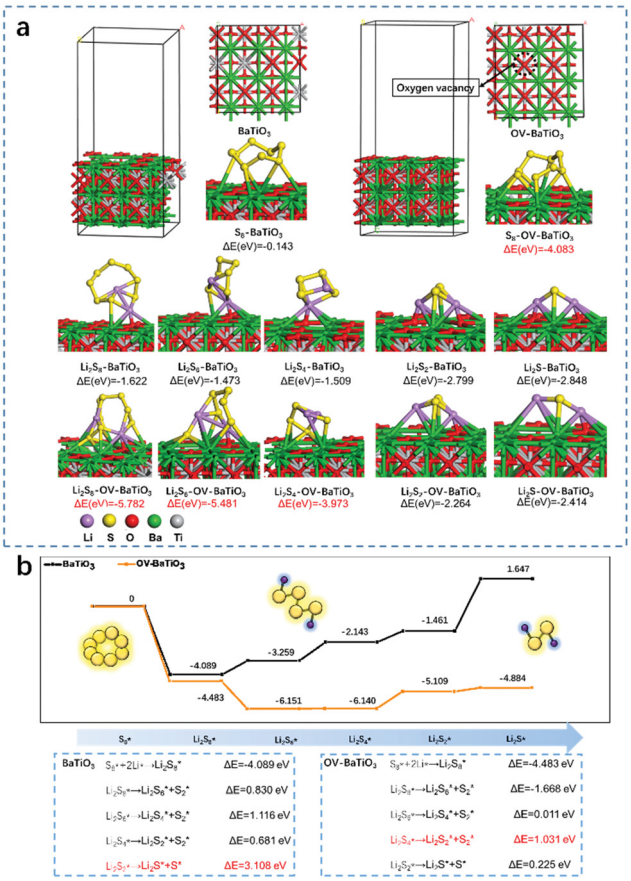

Fig. 3 (a) Density function theory (DFT) is employed to simulate the absorption energy of OV-$BaTiO_3$ and $BaTiO_3$ with different polysulfides. (b) The rate-limiting step of the whole conversion process on the OV-$BaTiO_3$ and $BaTiO_3$ based on DFT results.

energy of Li_2S_2, and Li_2S for OV-$BaTiO_3$ is lower than that of $BaTiO_3$; adsorption energies of $BaTiO_3$ for Li_2S_2 and Li_2S are −2.799 and −2.848 eV, respectively, which are much higher than that of OV-$BaTiO_3$. There was a widely held belief that shuttle effect involves soluble polysulfide ($Li_2S_{4\text{-}8}$), in which solid polysulfide ($Li_2S_{1\text{-}4}$) can be ignored.

Further analysis of the rate-limiting step and the calculation of adsorption energy involved is below (Fig. 3b):

$$\Delta E = E(\text{total}) - E(\text{slab}) - E\,(*)$$

Wherein, the adsorption of Li_2S_x is compared to the molecular energy of Li_2S_x in vacuum:

$$\Delta E\,(Li_2S_8) = E\,(Li_2S_8 + \text{slab}) - E\,(\text{slab}) - E\,(Li_2S_8)$$

The S_2/S of each desorption step is compared to the energy of the two Li_2S_x and the desorption of S_2:

$$Li_2S_4 \rightarrow Li_2S_2, \text{ then } S_2 = Li_2S_4 - Li_2S_2$$

$$\Delta E(S_2) = E(S_2 + \text{slab}) - E(\text{slab}) - E(Li_2S_4 - Li_2S_2)$$

$$Li_2S_4 \rightarrow Li_2S_2, \text{ then } S_2 = Li_2S_6 - Li_2S_4$$

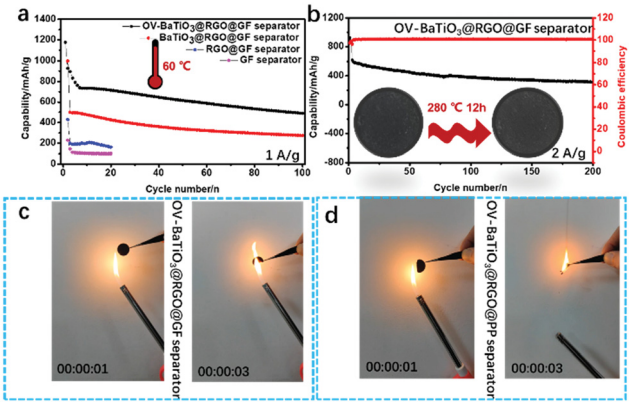

Fig. 4 (a) Cycling stability of OV-$BaTiO_3$@RGO@GF separator, $BaTiO_3$@RGO@GF separator, RGO@GF separator and GF separator at a current density of 1 A g^{-1} under a temperature of 60 °C. (b) Cycling stability of the OV-$BaTiO_3$@RGO@GF separator cycled at a current density of 2 A g^{-1} after heat treatment. The vertical firing test of the OV-$BaTiO_3$@RGO@GF separator (c) and OV-$BaTiO_3$@RGO@PP separator (d).

$$\Delta E(S_2) = E(S_2 + \text{slab}) - E(\text{slab}) - E(Li_2S_6 - Li_2S_4)$$

$$Li_2S_2 \rightarrow Li_2S, \text{ then } S = Li_2S_2 - Li_2S$$

$$\Delta E(S) = E(S + \text{slab}) - E(\text{slab}) - E\,(Li_2S_2 - Li_2S)$$

From here we can draw the conclusion that the rate-limiting step of a perfect surface of $BaTiO_3$ is Li_2S_2 desorption and S is 3.108 eV. Instead, the rate-limiting step of oxygen vacancies of OV-$BaTiO_3$ surface is 1.031 eV. Compared with the perfect surface, the reaction rate-limiting step is greatly reduced, so the formation of oxygen vacancies is conducive to the occurrence of reaction.

Although such design can be performed at a higher level at room temperature, we also need to think about the point of batteries' thermal safety characteristics.[37] For this reason, as we mentioned earlier, it is a good idea to use a higher temperature of the LSB. The oxygen vacancy of OV-$BaTiO_3$, conductive graphene, glass fiber skeleton of ternary composite structure, and the multicomponent integrated design can not only guarantee the coating fully maintaining its electrical conductivity, but also could effectively suppress the shuttle effect of polysulfide and ensure that the cycle stability of the battery can be maintained at 60 °C (Fig. 4a). The OV-$BaTiO_3$@RGO@GF separator maintained good charge and discharge stability under a current density of 1 A g^{-1} with a high capacity of 490 mA h g^{-1}. Further, the performance of battery using the GF separator is lower than that of any other modified separators because more polysulfides shuttle in the first few cycles. Next, the heat treatment with ultra-high temperature (280 °C) for OV-$BaTiO_3$@RGO@GF separator was tested and achieved good specific capacity (620 mA h g^{-1} at 2 A g^{-1}). Even more surprising, the battery remained safe after 200 cycles (Fig. 4b). From the images in Fig. 4b, there were no apparent changes of the OV-$BaTiO_3$@RGO@GF separator observed after the heat

treatment. On the contrary, the heat changes the OV-$BaTiO_3$@RGO@PP separator into carbon (Fig. S6, ESI†), which proves how reliable and good the OV-$BaTiO_3$@RGO@GF separator is. Further vertical firing tests are used to investigate the flame retardancy of the intumescent flame retardant on OV-$BaTiO_3$@RGO@GF separator and OV-$BaTiO_3$@RGO@PP separator (Fig. 4c and d), and the OV-$BaTiO_3$@RGO@GF separator shows good fire retardancy. These experimental results indicate that those properties of the coatings with OV-$BaTiO_3$ can reach the requirements of the weathering performance and fire retardancy of high performance LSB.

4. Conclusions

In this work, OV-$BaTiO_3$, an oxygen vacancy and ferroelectricity material, was applied as the coating of a separator for LSB, which effectively improved the discharge stability of LSB at high rate (10 A g^{-1}) and load (10 mg cm^{-2}). In addition, using this special material as a model, by first principles calculations an electrocatalyst related to the oxygen vacancy component adsorption of polysulfide is revealed and the performance is enhanced, and by using electrochemical experiments and *in situ* XRD, its advantages in the process of the reaction kinetics are proved. More importantly, the upper operating temperature limit of conventional LIB (60 °C) is overcome, which has the potential to reduce the risk of thermal runaway and simplify the thermal management of LSB. The work provides a technical choice for the design of a mixed glass fiber separator system for rechargeable LSB.

Conflicts of interest

There are no conflicts to declare.

Acknowledgements

We would like to thank the Analytical and Testing Center of Southwest Jiaotong University for the experimental analysis.

Notes and references

1 J. Lei, T. Liu, J. J. Chen, M. S. Zheng, Q. Zhang, B. W. Mao and Q. F. Dong, Exploring and Understanding the Roles of Li2Sn and the Strategies to beyond Present Li-S Batteries, *Chem*, 2020, **6**(10), 2533–2557.

2 M. Jana, R. Xu, X.-B. Cheng, J. S. Yeon, J. M. Park, J.-Q. Huang, Q. Zhang and H. S. Park, Rational design of two-dimensional nanomaterials for lithium–sulfur batteries, *Energy Environ. Sci.*, 2020, **13**(4), 1049–1075.

3 B. Ding, J. Wang, Z. Fan, S. Chen, Q. Lin, X. Lu, H. Dou, A. Kumar Nanjundan, G. Yushin, X. Zhang and Y. Yamauchi, Solid-state lithium–sulfur batteries: Advances, challenges and perspectives, *Mater. Today*, 2020, **40**, 114–131.

4 Z. Cheng, H. Pan, J. Chen, X. Meng and R. Wang, Separator Modified by Cobalt-Embedded Carbon Nanosheets Enabling Chemisorption and Catalytic Effects of Polysulfides for High-Energy-Density Lithium-Sulfur Batteries, *Adv. Energy Mater.*, 2019, **9**(32), 1901609.

5 S. Cheng, J. Wang, S. Duan, J. Zhang, Q. Wang, Y. Zhang, L. Li, H. Liu, Q. Xiao and H. Lin, Anionic oxygen vacancies in Nb2O5-/carbon hybrid host endow rapid catalytic behaviors for high-performance high areal loading lithium sulfur pouch cell, *Chem. Eng. J.*, 2021, **417**, 128172.

6 Z. Wei, Y. Ren, J. Sokolowski, X. Zhu and G. Wu, Mechanistic understanding of the role separators playing in advanced lithium-sulfur batteries, *InfoMat*, 2020, **2**(3), 483–508.

7 Y. Han, B. Liu, Z. Xiao, W. Zhang, X. Wang, G. Pan, Y. Xia, X. Xia and J. Tu, Interface issues of lithium metal anode for high-energy batteries: Challenges, strategies, and perspectives, *InfoMat*, 2021, **3**(2), 155–174.

8 H. Yao, K. Yan, W. Li, G. Zheng, D. Kong, Z. W. Seh, V. K. Narasimhan, Z. Liang and Y. Cui, Improved lithium–sulfur batteries with a conductive coating on the separator to prevent the accumulation of inactive S-related species at the cathode–separator interface, *Energy Environ. Sci.*, 2014, **7**(10), 3381–3390.

9 Y. Zhang, R. Wang, W. Tang, L. Zhan, S. Zhao, Q. Kang, Y. Wang and S. Yang, Efficient polysulfide barrier of a graphene aerogel–carbon nanofibers–Ni network for high-energy-density lithium–sulfur batteries with ultrahigh sulfur content, *J. Mater. Chem. A*, 2018, **6**(42), 20926–20938.

10 L. Wang, Z. Yang, H. Nie, C. Gu, W. Hua, X. Xu, X. a Chen, Y. Chen and S. Huang, A lightweight multifunctional interlayer of sulfur–nitrogen dual-doped graphene for ultrafast, long-life lithium–sulfur batteries, *J. Mater. Chem. A*, 2016, **4**(40), 15343–15352.

11 M. Chen, X. Zhao, Y. Li, P. Zeng, H. Liu, H. Yu, M. Wu, Z. Li, D. Shao, C. Miao, G. Chen, H. Shu, Y. Pei and X. Wang, Kinetically elevated redox conversion of polysulfides of lithium-sulfur battery using a separator modified with transition metals coordinated g-C3N4 with carbon-conjugated, *Chem. Eng. J.*, 2020, **385**, 123905.

12 F. Pei, L. L. Lin, A. Fu, S. G. Mo, D. H. Ou, X. L. Fang and N. F. Zheng, A Two-Dimensional Porous Carbon-Modified Separator for High-Energy-Density Li-S Batteries, *Joule*, 2018, **2**(2), 323–336.

13 Y. Z. Zhang, X. Ge, Q. Kang, Z. K. Kong, Y. L. Wang and L. Zhan, Vanadium oxide nanorods embed in porous graphene aerogel as high-efficiency polysulfide-trapping-conversion mediator for high performance lithium-sulfur batteries, *Chem. Eng. J.*, 2020, **393**, 124570.

14 F. Chen, X. Guan, H. Li, J. Ding, L. Zhu, B. Tang, V. Valtchev, Y. Yan, S. Qiu and Q. Fang, Three-Dimensional Radical Covalent Organic Frameworks as Highly Efficient and Stable Catalysts for Selective Oxidation of Alcohols, *Angew. Chem., Int. Ed.*, 2021, **60**(41), 22230–22235.

15 L. Ren, Q. Wang, Y. Li, C. Hu, Y. Zhao, L. Qiao, H. Zhou, W. Liu, H. Xu and X. Sun, Catalytic separators with Co–N–C

nanoreactors for high-performance lithium–sulfur batteries, *Inorg. Chem. Front.*, 2021, **8**(12), 3066–3076.

16 J. Xu, W. Tang, C. Yang, I. Manke, N. Chen, F. Lai, T. Xu, S. An, H. Liu, Z. Zhang, Y. Cao, N. Wang, S. Zhao, D. Niu and R. Chen, A Highly Conductive COF@CNT Electrocatalyst Boosting Polysulfide Conversion for Li–S Chemistry, *ACS Energy Lett.*, 2021, **6**(9), 3053–3062.

17 S. Bai, X. Liu, K. Zhu, S. Wu and H. Zhou, Metal–organic framework-based separator for lithium–sulfur batteries, *Nat. Energy*, 2016, **1**(7), 16094.

18 S. Li, J. Lin, Y. Ding, P. Xu, X. Guo, W. Xiong, D. Y. Wu, Q. Dong, J. Chen and L. Zhang, Defects Engineering of Lightweight Metal-Organic Frameworks-Based Electrocatalytic Membrane for High-Loading Lithium-Sulfur Batteries, *ACS Nano*, 2021, **15**(8), 13803–13813.

19 Z. Chang, Y. Qiao, J. Wang, H. Deng, P. He and H. Zhou, Fabricating better metal-organic frameworks separators for Li–S batteries: Pore sizes effects inspired channel modification strategy, *Energy Storage Mater.*, 2020, **25**, 164–171.

20 Q. Yang, Y. Liu, H. Ou, X. Li, X. Lin, A. Zeb and L. Hu, Fe-Based metal–organic frameworks as functional materials for battery applications, *Inorg. Chem. Front.*, 2022, **9**(5), 827–844.

21 T. Y. Lei, W. Chen, Y. Hu, W. Q. Lv, X. X. Lv, Y. C. Yan, J. W. Huang, Y. Jiao, J. W. Chu, C. Y. Yan, C. Y. Wu, Q. Li, W. D. He and J. Xiong, A Nonflammable and Thermotolerant Separator Suppresses Polysulfide Dissolution for Safe and Long-Cycle Lithium-Sulfur Batteries, *Adv. Energy Mater.*, 2018, **8**(32), 1802441.

22 Q. S. Wang, P. Ping, X. J. Zhao, G. Q. Chu, J. H. Sun and C. H. Chen, Thermal runaway caused fire and explosion of lithium ion battery, *J. Power Sources*, 2012, **208**, 210–224.

23 W. Zhang, Y. Liu and Z. Guo, Approaching high-performance potassium-ion batteries via advanced design strategies and engineering, *Sci. Adv.*, 2019, **5**(5), eaav7412.

24 Y.-F. Meng, H.-J. Liang, C.-D. Zhao, W.-H. Li, Z.-Y. Gu, M.-X. Yu, B. Zhao, X.-K. Hou and X.-L. Wu, Concurrent recycling chemistry for cathode/anode in spent graphite/LiFePO4 batteries: Designing a unique cation/anion-coworkable dual-ion battery, *J. Energy Chem.*, 2022, **64**, 166–171.

25 H. Zhu, Z. Li, F. Xu, Z. Qin, R. Sun, C. Wang, S. Lu, Y. Zhang and H. Fan, Ni3Se4@CoSe2 hetero-nanocrystals encapsulated into CNT-porous carbon interpenetrating frameworks for high-performance sodium ion battery, *J. Colloid Interface Sci.*, 2022, **611**, 718–725.

26 V. Chabot, D. Higgins, A. Yu, X. Xiao, Z. Chen and J. Zhang, A review of graphene and graphene oxide sponge: material synthesis and applications to energy and the environment, *Energy Environ. Sci.*, 2014, **7**(5), 1564.

27 M. Yang, Z. Sun, P. Nie, H. Yu, C. Zhao, M. Yu, Z. Luo, H. Geng and X. Wu, SbPS4: A novel anode for high-performance sodium-ion batteries, *Chin. Chem. Lett.*, 2022, **33**(1), 470–474.

28 Y. Xiang, L. Lu, A. G. P. Kottapalli and Y. Pei, Status and perspectives of hierarchical porous carbon materials in terms of high-performance lithium–sulfur batteries, *Carbon Energy*, 2022, **4**(3), 346–398.

29 K. Xie, Y. You, K. Yuan, W. Lu, K. Zhang, F. Xu, M. Ye, S. Ke, C. Shen, X. Zeng, X. Fan and B. Wei, Ferroelectric-Enhanced Polysulfide Trapping for Lithium-Sulfur Battery Improvement, *Adv. Mater.*, 2017, **29**(6), 1604724.

30 R. Saroha, J. Heo, X. Li, N. Angulakshmi, Y. Lee, H. J. Ahn, J. H. Ahn and J. H. Kim, Asymmetric separator integrated with ferroelectric-BaTiO3 and mesoporous-CNT for the reutilization of soluble polysulfide in lithium-sulfur batteries, *J. Alloys Compd.*, 2022, **893**, 162272.

31 Z. Li, C. Zhou, J. Hua, X. Hong, C. Sun, H. W. Li, X. Xu and L. Mai, Engineering Oxygen Vacancies in a Polysulfide-Blocking Layer with Enhanced Catalytic Ability, *Adv. Mater.*, 2020, **32**(10), 1907444.

32 J. Wang, W. Qin, X. Zhu and Y. Teng, Covalent organic frameworks (COF)/CNT nanocomposite for high performance and wide operating temperature lithium–sulfur batteries, *Energy*, 2020, **199**, 117372.

33 L. Wang, Z.-Y. Wang, J.-F. Wu, G.-R. Li, S. Liu and X.-P. Gao, To effectively drive the conversion of sulfur with electroactive niobium tungsten oxide microspheres for lithium−sulfur battery, *Nano Energy*, 2020, **77**, 105173.

34 J. He, A. Bhargav and A. Manthiram, High-Energy-Density, Long-Life Lithium-Sulfur Batteries with Practically Necessary Parameters Enabled by Low-Cost Fe-Ni Nanoalloy Catalysts, *ACS Nano*, 2021, **15**(5), 8583–8591.

35 H. J. Peng, J. Q. Huang, X. B. Cheng and Q. Zhang, Review on High-Loading and High-Energy Lithium-Sulfur Batteries, *Adv. Energy Mater.*, 2017, **7**(24), 1700260.

36 Q. He, B. Yu, Z. H. Li and Y. Zhao, Density Functional Theory for Battery Materials, *Energy Environ. Mater.*, 2019, **2**(4), 264–279.

37 D. S. Ren, H. J. Hsu, R. H. Li, X. N. Feng, D. X. Guo, X. B. Han, L. G. Lu, X. M. He, S. Gao, J. X. Hou, Y. Li, Y. L. Wang and M. G. Ouyang, A comparative investigation of aging effects on thermal runaway behavior of lithium-ion batteries, *eTransportation*, 2019, **2**, 100034.